

Article

Synthesis of $Y_3Al_5O_{12}:Ce$ Powders for X-ray Luminescent Diamond Composites

Sergey V. Kuznetsov ^{1,*}, Vadim S. Sedov ¹, Artem K. Martyanov ¹, Dmitrii S. Vakalov ², Ludmila V. Tarala ², Ivan A. Tiazhelov ¹ and Kirill N. Boldyrev ³

¹ Prokhorov General Physics Institute of the Russian Academy of Sciences, 119991 Moscow, Russia

² Scientific and Laboratory Complex Clean Room, North Caucasus Federal University, 355009 Stavropol, Russia

³ Institute of Spectroscopy of the Russian Academy of Sciences, Troitsk, 108840 Moscow, Russia

* Correspondence: kouznetzovsv@gmail.com

Abstract: A concentration series of $Y_3Al_5O_{12}:Ce$ solid solutions were prepared, and the composition demonstrating the highest X-ray luminescence intensity of cerium was identified. Based on the best composition, a series of luminescent diamond- $Y_3Al_5O_{12}:Ce$ composite films were synthesized using microwave plasma-assisted chemical vapor deposition (CVD) in methane–hydrogen gas mixtures. Variations in the amounts of the embedded $Y_3Al_5O_{12}:Ce$ powders allowed for the fine-tuning of the luminescence intensity of the composite films.

Keywords: yttrium–aluminum garnet; cerium; diamond composite; X-ray luminescence



Citation: Kuznetsov, S.V.; Sedov, V.S.; Martyanov, A.K.; Vakalov, D.S.; Tarala, L.V.; Tiazhelov, I.A.; Boldyrev, K.N. Synthesis of $Y_3Al_5O_{12}:Ce$ Powders for X-ray Luminescent Diamond Composites. *Inorganics* **2022**, *10*, 240. <https://doi.org/10.3390/inorganics10120240>

Academic Editor: Rainer Niewa

Received: 9 November 2022

Accepted: 30 November 2022

Published: 5 December 2022

Publisher's Note: MDPI stays neutral with regard to jurisdictional claims in published maps and institutional affiliations.



Copyright: © 2022 by the authors. Licensee MDPI, Basel, Switzerland. This article is an open access article distributed under the terms and conditions of the Creative Commons Attribution (CC BY) license (<https://creativecommons.org/licenses/by/4.0/>).

1. Introduction

Diamond photonics based on impurity atom-vacancy optical centers is being intensively studied for applications in biomedical applications [1,2], thermometry [3–5], single-photon emitters [6–8], and X-ray optics [9–12]. Specifically, great potential lies in the combination of the properties of pristine diamond with the rich luminescent properties of rare earth (RE) elements. There are several approaches to reaching this goal by obtaining RE-doped diamond materials using both chemical vapor deposition (CVD) and high-pressure high-temperature (HPHT) processes; however, without any major breakthroughs to obtain highly luminescent diamonds [13–18]. A new emerging path is the formation of luminescent composites based on synthetic diamonds with embedded luminescent RE-based nanoparticles [9], which already possess the targeted luminescent properties.

In the first works on such diamond-RE composites [11,12,19–21], the following compounds were tested as the materials for the luminescent particles: EuF_3 , β - $NaGdF_4:Eu$, $Gd_3Al_5O_{12}:Sc:Ce$, and $Y_3Al_5O_{12}:Ce$ nanoparticles. Summarizing all of these works, the highest X-ray luminescence (XRL) so far was achieved using nanopowders of $[Y_{2.98}Ce_{0.02}]\{Al_2\}Al_3O_{12}$ [21]. These composites are of interest for imaging intense high-energy X-ray fluxes, such as those in various synchrotrons and free-electron lasers. The literature presents various data on the concentrations of cerium in solid solutions based on yttrium–aluminum garnets, but often the concentration of cerium is presented in unclear values, percentages, or fractions, while the type of values is not indicated, e.g., molar, weight, atomic, or formula units [22–24]. Earlier, in our preliminary study, on the basis of a concentration series of powders of solid solutions (without integration into diamond films), the boundaries of the existence of single-phase solid solutions were revealed, and the compositions demonstrating the highest luminescence intensity were estimated. However, the optimal compound for maximizing the XRL intensity of the diamond composite may vary from the optimal compound of pristine RE powder. In addition, to achieve the lateral uniformity of the XRL signal from the composite film, it is necessary to carry out a synthesis with a smaller particle size. As a result, the aim of this work was to identify the composition

that demonstrates the highest intensity of X-ray luminescence and to create an effective luminescent composite based on it.

2. Results

The powder synthesis of the concentration series $Y_{3-x}Ce_xAl_5O_{12}$ was carried out by spraying a solution of cerium nitrate, aluminum, and yttrium chlorides in a 25% solution of ammonia, taken with a 6-fold excess, and ammonium sulfate (0.45 M). The cerium concentration was varied from $x = 0.0100$ f.u. to 0.0250 f.u., which corresponds to the interval from 0.33(3) to 0.83(3) at%. (Table 1). The resulting slurry was washed with ammonium sulfate solution (0.045 M). The washed precipitate was dried in an oven at 60 °C for 15 h. The dried precipitate was calcined in a Nabertherm 08/18 furnace in corundum crucibles at 1460 °C for 4 h.

Table 1. Compositions and characteristics of the synthesized samples.

Sample	a , Å	CSR Size, nm	DTA, °C
PKS-01— $Y_{2.9900}Ce_{0.0100}Al_5O_{12}$	12.013 ± 0.002	221	968.0
PKS-02— $Y_{2.9875}Ce_{0.0125}Al_5O_{12}$	12.015 ± 0.002	178	968.0
PKS-03— $Y_{2.9850}Ce_{0.0150}Al_5O_{12}$	12.014 ± 0.002	193	972.8
PKS-04— $Y_{2.9825}Ce_{0.0175}Al_5O_{12}$	12.014 ± 0.002	193	971.8
PKS-05— $Y_{2.9800}Ce_{0.0200}Al_5O_{12}$	12.014 ± 0.002	180	974.4
PKS-06— $Y_{2.9775}Ce_{0.0225}Al_5O_{12}$	12.014 ± 0.002	169	974.7
PKS-07— $Y_{2.9750}Ce_{0.0250}Al_5O_{12}$	12.015 ± 0.002	>250	970.3

According to the differential thermal analysis (DTA), the garnet phase for the entire concentration range was formed at a temperature ≈ 970 °C (see Figure 1 for the DTA of the PKS-06 sample). The recorded temperature corresponds to the temperature of the phase transition of a mixture of amorphous oxides into the garnet phase [25,26].

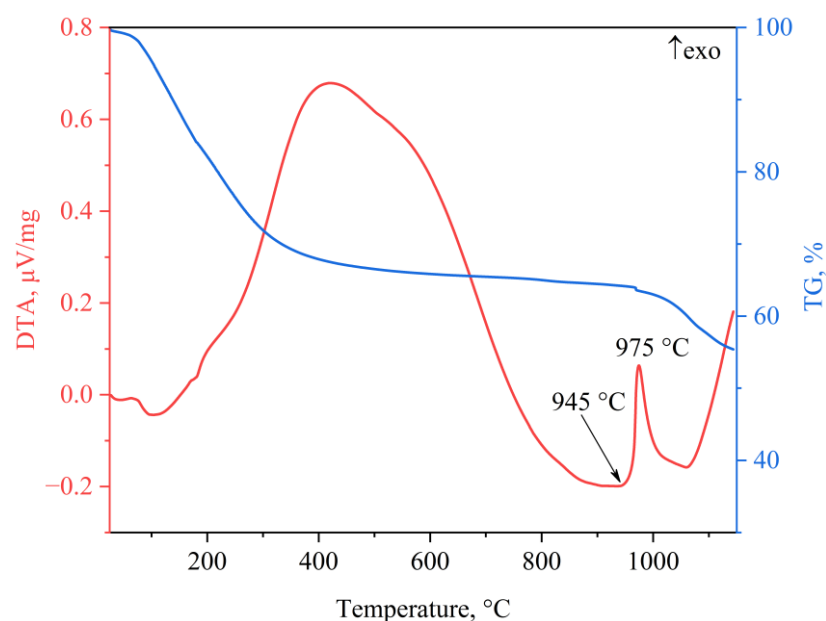


Figure 1. Typical DTA-TG for the PKS-06 sample.

According to the X-ray phase analysis of the samples after calcination at a temperature of 1460 °C for 4 h, single-phase samples with a garnet structure were synthesized (Figure 2). Based on the X-ray data, the lattice parameters and the sizes of the coherent scattering

regions (CSRs) were calculated (Table 1). Due to the low concentrations of cerium, the changes in the lattice parameters were comparable with the error of the synthesis experiment of $\Delta a = \pm 0.002 \text{ \AA}$. As follows from the data presented in Table 1, the CSR values are in the range of 169–221 nm, while any dependence on the composition of the samples is not traced.

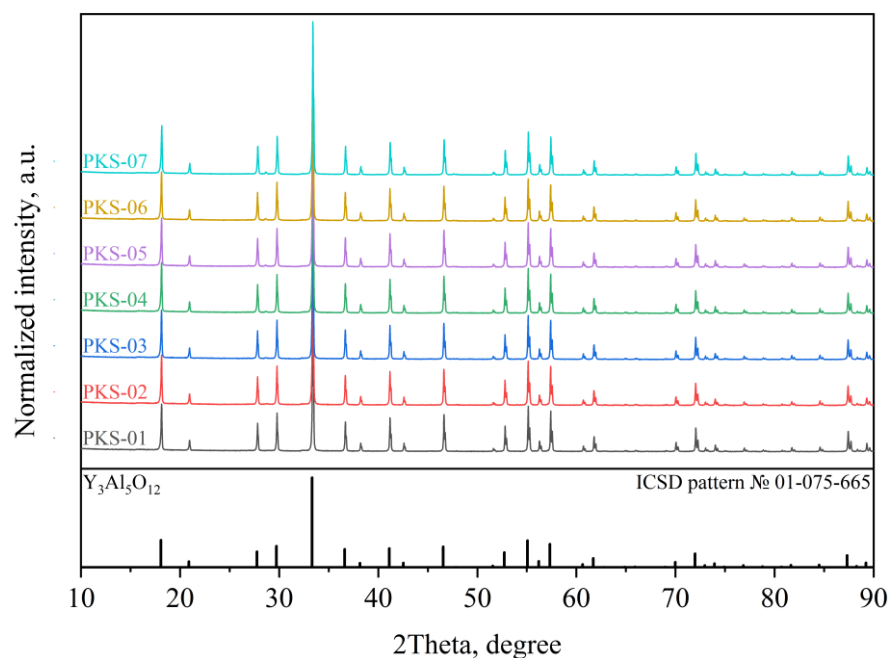


Figure 2. X-ray diffraction patterns of the YAG:Ce samples synthesized at 1460 °C.

The SEM studies of the samples indicated that the as-synthesized YAG:Ce powders consisted of micrometer-sized particle agglomerates (Figure 3). The sizes of the separate particles are $\approx 200\text{--}300 \text{ nm}$, which correlates well with the measured size of the CSRs.

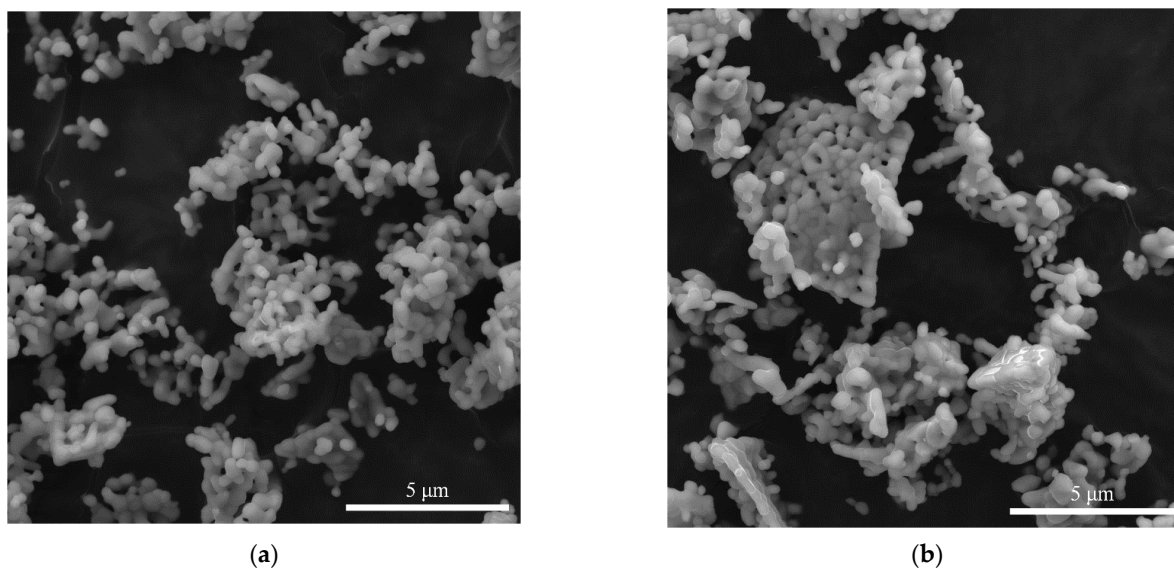


Figure 3. Cont.

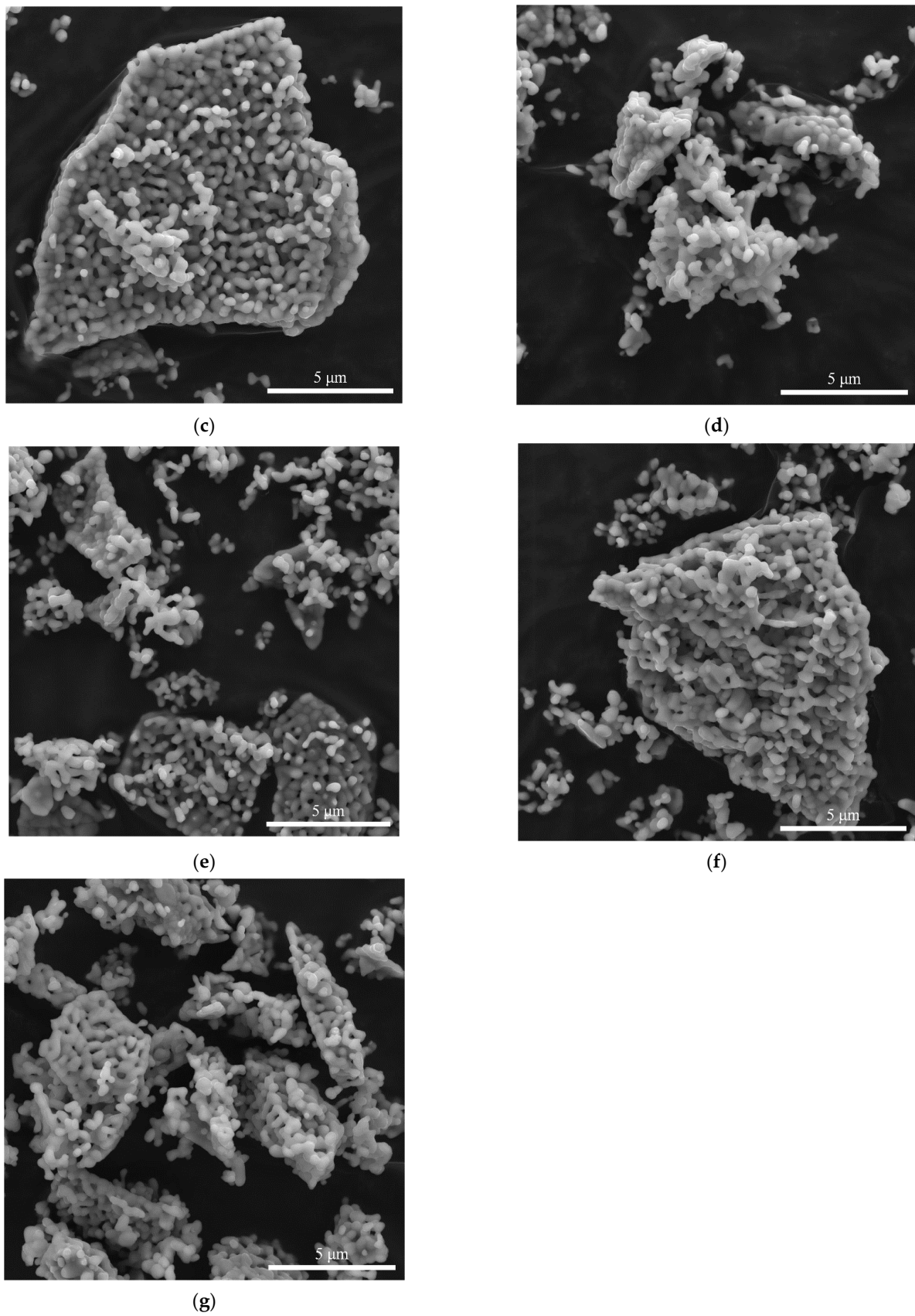


Figure 3. SEM of the YAG:Ce samples synthesized at 1460 °C. (a) PKS-01. (b) PKS-02. (c) PKS-03. (d) PKS-04. (e) PKS-05. (f) PKS-06. (g) PKS-07.

Studies of the X-ray luminescence of the $Y_{3-x}Ce_xAl_5O_{12}:Ce$ samples under X-ray excitation, $k_{\alpha(Ag)} = 22.16$ keV, showed (Figure 4) that the luminescence maximum is in the region of 530 nm. At the same time, when the cerium concentration increased from 0.0100 to 0.0225 f.u., the intensity increased, and upon reaching $x = 0.0250$ f.u., it decreased. In addition, as shown in the inset to Figure 4, a slight shift in the spectra was recorded as the cerium concentration increased. The detected effect of the shift of the X-ray luminescence maxima is in good agreement with the data presented in [22], where the shift of the photoluminescence (PL) maxima to higher wavelengths is shown with an increase in the cerium concentration from 0.006 to 0.210 f.u. The shift of the luminescence band maximum resulted from the replacement of yttrium by the heavier cerium and a smooth change in the energy of the phonon matrix [27].

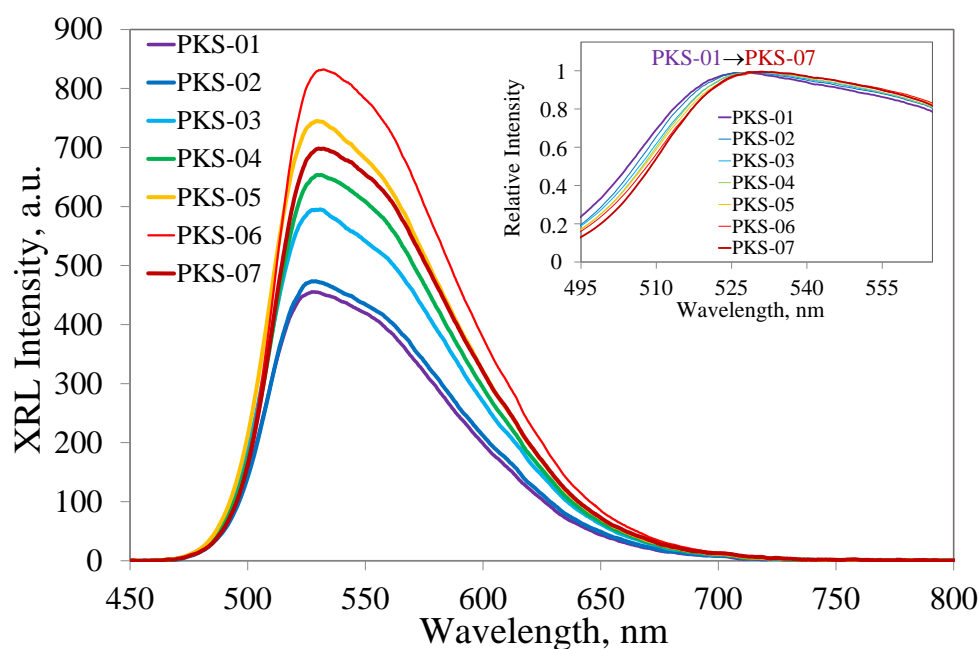


Figure 4. X-ray luminescence spectra of the concentration series samples. Inset—XRL spectra of the concentration series samples, which are reduced/normalized to unity to visualize the shift in the position of the maximum of the luminescence band.

Based on the particles of the $Y_{2.9775}Ce_{0.0225}Al_5O_{12}$ composition, suspensions in DMSO with a concentration of 10 mg/mL were prepared, which were then sequentially deposited dropwise on a diamond substrate, according to the protocol described in [9]. The typical SEM image of the obtained film is shown in Figure 5a. The structure of the composite film was similar to the structure of the microcrystalline diamond films, with a grain size of a few micrometers. As a result, four samples were obtained with one, two, three, and four drops of powder suspension on identical samples. A registration of the PL spectra upon excitation at a wavelength of 473 nm (LabRam HR840) was carried out using the same 50-point pattern on the surface of each sample, followed by averaging the results (Figure 5b). A registration of the XRL spectra on an excitation X-ray tube with a silver anode operating was carried out (Figure 5c). As a result, an increase in the intensity of the X-ray and photoluminescence was observed with an increase in the number of deposited particles, which makes it possible to develop efficient luminescence materials based on diamond-particle composites.

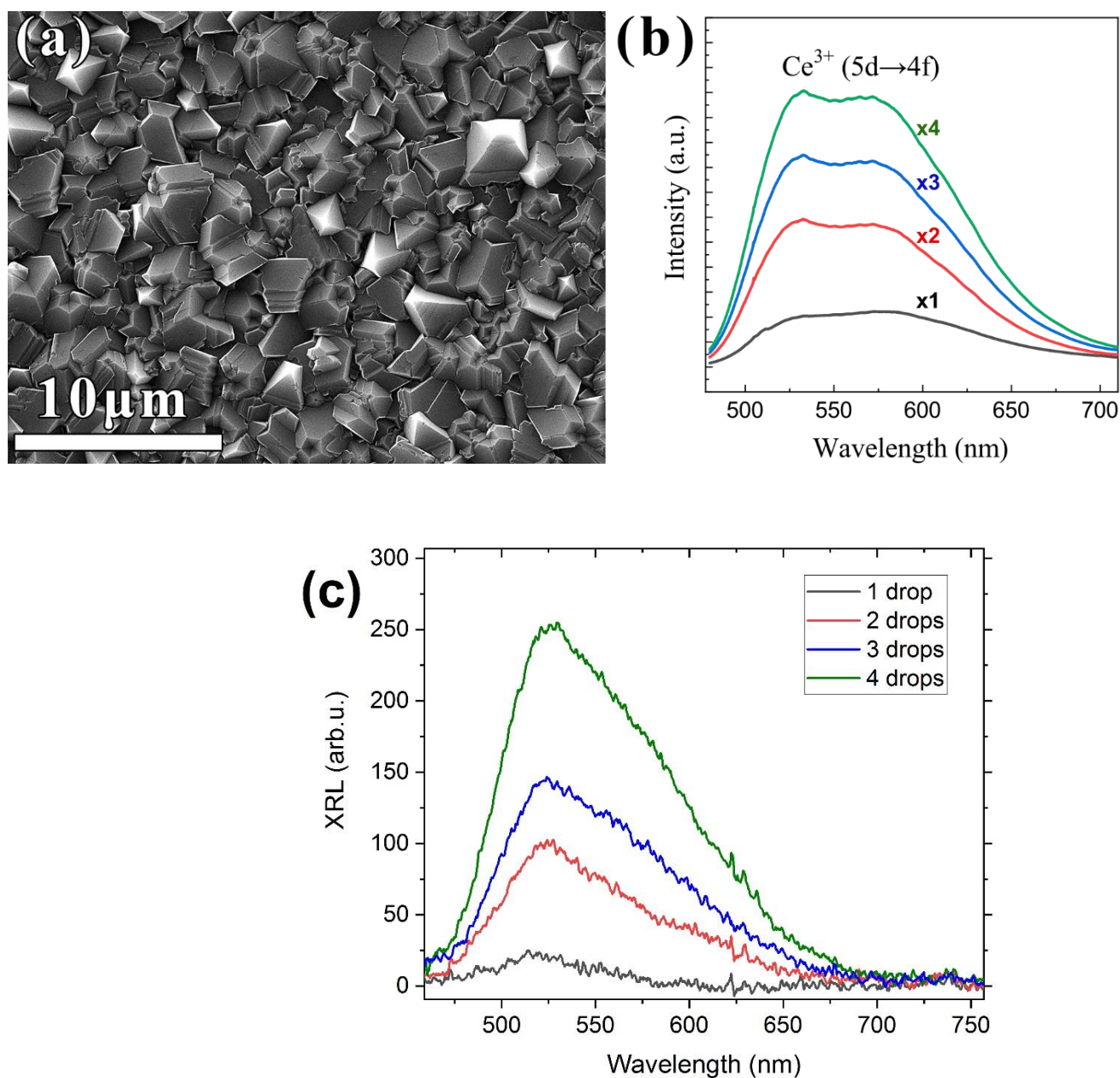


Figure 5. SEM images of the surface of a diamond- $\text{Y}_3\text{Al}_5\text{O}_{12}:\text{Ce}$ composite film prepared with four drops of powder suspension (a), PL (b), and XRL (c) spectra of a series of composite films prepared using similar procedures but with one, two, three, and four drops of suspension.

3. Materials and Methods

The precursors for the powder synthesis were as follows: cerium nitrate hexahydrate (99.0%, Vecton, St. Petersburg, Russia), aluminum chloride hexahydrate (99.9%, Lanhit Ltd., Moscow, Russia), yttrium chloride hexahydrate (99.99%, Lanhit Ltd., Moscow, Russia), ammonia (99.999%, Stavreakhim Ltd., Stavropol, Russia), ammonium sulfate (99.0%, Component Reactiv Ltd., Moscow, Russia), and deionized water. All of the initial reagents were used without additional purification steps.

The thermal behavior of the powders was determined using a synchronous thermal analysis instrument (STA, 449 F1 Jupiter, Netzsch, Karlsruhe, Germany) in the temperature range between 27 and 1150 °C and with a heating rate of 25 °C/min. The powder diffraction patterns were recorded using an X-ray diffractometer (XRD, Empyrean, Panalytical, Almelo, The Netherlands) equipped with an X-ray tube with a copper anode ($\text{CuK}\alpha 1$, $\lambda = 1.5406\ \text{\AA}$).

over a 2θ angle range between 10 and 90° , a step of 0.01° , and a scanning speed of $0.7^\circ/\text{min}$. Phase identification and full-profile analysis of the X-ray diffraction patterns by the Rietveld method were carried out using the Highscore Plus software with the ICDD PDF-2 database. Micrographs of the ceramic powders and composite films were taken with a scanning electron microscope (SEM, microscope LM Mira 3, Tescan, Brno, Czech Republic). Raman and photoluminescence spectra of the diamond composites were taken at room temperature with a LabRam HR840 (Horiba Jobin-Yvon, Stow, MA, USA) spectrometer in a confocal configuration. The laser beam with a wavelength of 473 nm was focused in an $\approx 1 \mu\text{m}$ spot on the sample surface. The XRL spectra of the powders were recorded at room temperature on an Ocean Insight Ocean HDX VIS-NIR fiber-optic spectrometer in the range of 350–1100 nm with a resolution of 0.7 nm under excitation by an X-ray tube with a silver anode operating at a voltage of 40 kV and a current of 35 mA with an X-ray photon energy of about 22 keV.

The diamond composites were formed in two steps by microwave plasma chemical vapor deposition (ARDIS-100, 2.45 GHz, Optosystems LLC, Moscow, Russia) [28] in hydrogen–methane gas mixtures. First, 3 μm -thick polycrystalline diamond films were grown on (100) silicon $10 \times 10 \times 1 \text{ mm}^3$ plates. These layers were used as substrates for applying the $\text{Y}_3\text{Al}_5\text{O}_{12}:\text{Ce}$ suspensions. A required number of drops (1–4, 0.02 mL each) of the suspensions of $\text{Y}_3\text{Al}_5\text{O}_{12}:\text{Ce}$ in dimethyl sulfoxide (DMSO, 10 mg/mL) were applied one-by-one on the first diamond layer. Each droplet was dried separately using an SPS SPIN 150 spin coater (3000 rpm, 5 min). Additionally, the Ce-contained powders were covered with a non-coalesced layer of nanodiamond particles (the particle sizes were 3–7 nm, Zeta potential $> +50\text{mV}$, Cardiff University [29,30]), which became additional nucleation centers for the second CVD diamond layer and, at the same time, provided protection for the RE powders from being etched by atomic hydrogen in the CVD process. The 2 μm -thick diamond layer grown in the second CVD step encapsulated the applied nanoparticles to form a “Diamond– $\text{Y}_3\text{Al}_5\text{O}_{12}:\text{Ce}$ ” composite. The growth conditions for all of the polycrystalline diamond films were as follows: the total gas flow was 500 sccm; the methane content was 4% CH_4/H_2 ; the pressure was 75 torr; the microwave power was 4.5 kW; the standard deposition rate was 1 $\mu\text{m}/\text{hour}$. The substrate temperature was maintained at $840 \pm 20^\circ\text{C}$, as measured by a two-color pyrometer METIS M322 (SensorTherm GmbH, Moscow, Russia).

4. Conclusions

A concentration series of $\text{Y}_{3-x}\text{Ce}_x\text{Al}_5\text{O}_{12}$ solid solutions with a cerium concentration of $x = 0.0100$ f.u. were synthesized to 0.0250 f.u. The crystallization of the garnet phase for the synthesized solid solutions occurs at a temperature of about 970°C . The subsequent high-temperature treatment at a temperature of 1460°C for 4 h led to the synthesis of particles with a size of about 200–300 nm, which were combined into agglomerates with a size of about one micron. Based on the X-ray luminescence spectra, the composition of $\text{Y}_{2.9775}\text{Ce}_{0.0225}\text{Al}_5\text{O}_{12}$ was revealed, which demonstrates the highest luminescence intensity. An increase in the intensity of the photoluminescence and an increase in the number of the deposited nanoparticles were revealed. As a result, the composites based on the diamond– $\text{Y}_{2.9775}\text{Ce}_{0.0225}\text{Al}_5\text{O}_{12}$ with a four-stage particle deposition procedure demonstrated the highest photoluminescence. The developed composites are promising for the visualization of high-power X-ray and synchrotron beams.

Author Contributions: Conceptualization, S.V.K. and V.S.S.; methodology, A.K.M.; validation, S.V.K.; investigation, D.S.V., L.V.T., I.A.T. and K.N.B.; resources, S.V.K. and V.S.S.; writing—original draft preparation, S.V.K., V.S.S. and A.K.M.; writing—review and editing, S.V.K., V.S.S. and A.K.M. All authors have read and agreed to the published version of the manuscript.

Funding: The study was supported by Russian Science Foundation grant No. 22-13-00401, <https://rscf.ru/en/project/22-13-00401/>.

Data Availability Statement: Not applicable.

Acknowledgments: The YAG: Ce samples were partially characterized by using equipment from the Center for Collective Use of the North Caucasus Federal University.

Conflicts of Interest: The authors declare no conflict of interest.

References

1. Nunn, N.; Shames, A.I.; Torelli, M.; Smirnov, A.I.; Shenderova, O. Luminescent Diamond: A Platform for Next Generation Nanoscale Optically Driven Quantum Sensors. In *Luminescent Nanomaterials*; Jenny Stanford Publishing: Dubai, United Arab Emirates, 2022; pp. 1–95.
2. Firestein, R.; Marcinkiewicz, C.; Nie, L.; Chua, H.K.; Quesada, I.V.; Torelli, M.; Sternberg, M.; Gligorijevic, B.; Shenderova, O.; Schirhagl, R. Pharmacodynamic Studies of Fluorescent Diamond Carriers of Doxorubicin in Liver Cancer Cells and Colorectal Cancer Organoids. *Nanotechnol. Sci. Appl.* **2021**, *14*, 139. [[CrossRef](#)] [[PubMed](#)]
3. Romshin, A.M.; Zeeb, V.; Martyanov, A.K.; Kudryavtsev, O.S.; Pasternak, D.G.; Sedov, V.S.; Ralchenko, V.G.; Sinogeykin, A.G.; Vlasov, I.I. A New Approach to Precise Mapping of Local Temperature Fields in Submicrometer Aqueous Volumes. *Sci. Rep.* **2021**, *11*, 14228. [[CrossRef](#)] [[PubMed](#)]
4. Alkahtani, M.; Cojocar, I.; Liu, X.; Herzig, T.; Meijer, J.; Küpper, J.; Lühmann, T.; Akimov, A.V.; Hemmer, P.R. Tin-Vacancy in Diamonds for Luminescent Thermometry. *Appl. Phys. Lett.* **2018**, *112*, 241902. [[CrossRef](#)]
5. Nguyen, C.T.; Evans, R.E.; Sipahigil, A.; Bhaskar, M.K.; Sukachev, D.D.; Agafonov, V.N.; Davydov, V.A.; Kulikova, L.F.; Jelezko, F.; Lukin, M.D. All-Optical Nanoscale Thermometry with Silicon-Vacancy Centers in Diamond. *Appl. Phys. Lett.* **2018**, *112*, 203102. [[CrossRef](#)]
6. Aharonovich, I.; Castelletto, S.; Simpson, D.A.; Su, C.-H.; Greentree, A.D.; Prawer, S. Diamond-Based Single-Photon Emitters. *Rep. Prog. Phys.* **2011**, *74*, 076501. [[CrossRef](#)]
7. Lenzini, F.; Gruhler, N.; Walter, N.; Pernice, W.H. Diamond as a Platform for Integrated Quantum Photonics. *Adv. Quantum Technol.* **2018**, *1*, 1800061. [[CrossRef](#)]
8. Kurochkin, N.S.; Savinov, S.A.; Bi, D.; Sychev, V.V.; Eliseev, S.P.; Gritsienko, A.V. Characterization of Milled High-Pressure High-Temperature NV-Center Nanodiamonds for Single-Photon Source Applications. *J. Russ. Laser Res.* **2021**, *42*, 713–720. [[CrossRef](#)]
9. Sedov, V.; Kuznetsov, S.; Martyanov, A.; Ralchenko, V. Luminescent Diamond Composites. *Funct. Diam.* **2022**, *2*, 53–63. [[CrossRef](#)]
10. Osadchy, A.V.; Vlasov, I.I.; Kudryavtsev, O.S.; Sedov, V.S.; Ralchenko, V.G.; Batygov, S.H.; Savin, V.V.; Ershov, P.A.; Chaika, V.A.; Narikov, A.S.; et al. Luminescent Diamond Window of the Sandwich Type for X-ray Visualization. *Appl. Phys. A* **2018**, *124*, 807. [[CrossRef](#)]
11. Sedov, V.; Kouznetsov, S.; Martyanov, A.; Proydakova, V.; Ralchenko, V.; Khomich, A.; Voronov, V.; Batygov, S.; Kamenskikh, I.; Spassky, D.; et al. Diamond–Rare Earth Composites with Embedded NaGdF₄:Eu Nanoparticles as Robust Photo- and X-ray-Luminescent Materials for Radiation Monitoring Screens. *ACS Appl. Nano Mater.* **2020**, *3*, 1324–1331. [[CrossRef](#)]
12. Sedov, V.; Kuznetsov, S.; Kamenskikh, I.; Martyanov, A.; Vakalov, D.; Savin, S.; Rubtsova, E.; Tarala, V.; Omelkov, S.; Kotlov, A.; et al. Diamond Composite with Embedded YAG:Ce Nanoparticles as a Source of Fast X-ray Luminescence in the Visible and near-IR Range. *Carbon* **2021**, *174*, 52–58. [[CrossRef](#)]
13. Vanpoucke, D.E.; Nicley, S.S.; Raymakers, J.; Maes, W.; Haenen, K. Can Europium Atoms Form Luminescent Centres in Diamond: A Combined Theoretical–Experimental Study. *Diam. Relat. Mater.* **2019**, *94*, 233–241. [[CrossRef](#)]
14. Palyanov, Y.N.; Borzdov, Y.M.; Khokhryakov, A.F.; Kupriyanov, I.N. High-Pressure Synthesis and Characterization of Diamond from Europium Containing Systems. *Carbon* **2021**, *182*, 815–824. [[CrossRef](#)]
15. Cajzl, J.; Akhetova, B.; Nekvindová, P.; Macková, A.; Malinský, P.; Oswald, J.; Remeš, Z.; Varga, M.; Kromka, A. Co-Implantation of Er and Yb Ions into Single-Crystalline and Nano-Crystalline Diamond. *Surf. Interface Anal.* **2018**, *50*, 1218–1223. [[CrossRef](#)]
16. Ekimov, E.A.; Zibrov, I.P.; Malykhin, S.A.; Khmel'nitskiy, R.A.; Vlasov, I.I. Synthesis of Diamond in Double Carbon-Rare Earth Element Systems. *Mater. Lett.* **2017**, *193*, 130–132. [[CrossRef](#)]
17. Khokhryakov, A.F.; Borzdov, Y.M.; Kupriyanov, I.N. High-Pressure Diamond Synthesis in the Presence of Rare-Earth Metals. *J. Cryst. Growth* **2020**, *531*, 125358. [[CrossRef](#)]
18. Magyar, A.; Hu, W.; Shanley, T.; Flatté, M.E.; Hu, E.; Aharonovich, I. Synthesis of Luminescent Europium Defects in Diamond. *Nat. Commun.* **2014**, *5*, 1–6. [[CrossRef](#)]
19. Sedov, V.S.; Kuznetsov, S.V.; Ralchenko, V.G.; Mayakova, M.N.; Krivobok, V.S.; Savin, S.S.; Zhuravlev, K.P.; Martyanov, A.K.; Romanishkin, I.D.; Khomich, A.A. Diamond-EuF₃ Nanocomposites with Bright Orange Photoluminescence. *Diam. Relat. Mater.* **2017**, *72*, 47–52. [[CrossRef](#)]
20. Kuznetsov, S.V.; Sedov, V.S.; Martyanov, A.K.; Batygov, S.C.; Vakalov, D.S.; Boldyrev, K.N.; Tiazhelov, I.A.; Popovich, A.F.; Pasternak, D.G.; Bland, H.; et al. Cerium-Doped Gadolinium-Scandium-Aluminum Garnet Powders: Synthesis and Use in X-ray Luminescent Diamond Composites. *Ceram. Int.* **2022**, *48*, 12962–12970. [[CrossRef](#)]
21. Kuznetsov, S.V.; Sedov, V.S.; Martyanov, A.K.; Batygov, S.C.; Vakalov, D.S.; Savin, S.S.; Tarala, V.A. X-ray Luminescence of Diamond Composite Films Containing Yttrium-Aluminum Garnet Nanoparticles with Varied Composition of Sc–Ce Doping. *Ceram. Int.* **2021**, *47*, 13922–13926. [[CrossRef](#)]

22. Nakamura, H.; Shinozaki, K.; Okumura, T.; Nomura, K.; Akai, T. Massive Red Shift of Ce³⁺ in Y₃Al₅O₁₂ Incorporating Super-High Content of Ce. *RSC Adv.* **2020**, *10*, 12535–12546. [[CrossRef](#)] [[PubMed](#)]
23. Cantarano, A.; Testemale, D.; Homeyer, E.; Okuno, H.; Potdevin, A.; Dujardin, C.; Ibanez, A.; Dantelle, G. Drastic Ce³⁺ Insertion Enhancement in YAG Garnet Nanocrystals through a Solvothermal Route. *Front. Mater.* **2021**, *8*, 768087. [[CrossRef](#)]
24. Kwon, S.B.; Choi, S.H.; Yoo, J.H.; Jeong, S.G.; Song, Y.H.; Yoon, D.H. Synthesis Design of Y₃Al₅O₁₂: Ce³⁺ Phosphor for Fabrication of Ceramic Converter in Automotive Application. *Opt. Mater.* **2018**, *80*, 265–270. [[CrossRef](#)]
25. Matsushita, N.; Tsuchiya, N.; Nakatsuka, K.; Yanagitani, T. Precipitation and Calcination Processes for Yttrium Aluminum Garnet Precursors Synthesized by the Urea Method. *J. Am. Ceram. Soc.* **1999**, *82*, 1977–1984. [[CrossRef](#)]
26. Li, X.; Zheng, B.; Odoom-Wubah, T.; Huang, J. Co-Precipitation Synthesis and Two-Step Sintering of YAG Powders for Transparent Ceramics. *Ceram. Int.* **2013**, *39*, 7983–7988. [[CrossRef](#)]
27. Lin, Y.-C.; Erhart, P.; Bettinelli, M.; George, N.C.; Parker, S.F.; Karlsson, M. Understanding the Interactions between Vibrational Modes and Excited State Relaxation in Y_{3-x}Ce_xAl₅O₁₂: Design Principles for Phosphors Based on 5d–4f Transitions. *Chem. Mater.* **2018**, *30*, 1865–1877. [[CrossRef](#)]
28. Sedov, V.S.; Martyanov, A.K.; Khomich, A.A.; Savin, S.S.; Zavedeev, E.V.; Ralchenko, V.G. Deposition of Diamond Films on Si by Microwave Plasma CVD in Varied CH₄-H₂ Mixtures: Reverse Nanocrystalline-to-Microcrystalline Structure Transition at Very High Methane Concentrations. *Diam. Relat. Mater.* **2020**, *109*, 108072. [[CrossRef](#)]
29. Ginés, L.; Mandal, S.; Ashek-I-Ahmed; Cheng, C.-L.; Sow, M.; Williams, A.O. Positive Zeta Potential of Nanodiamonds. *Nanoscale* **2017**, *9*, 12549–12555. [[CrossRef](#)]
30. Mandal, S. Nucleation of Diamond Films on Heterogeneous Substrates: A Review. *RSC Adv.* **2021**, *11*, 10159–10182. [[CrossRef](#)]